TRANSACTIONS OF THE INSTITUTE OF MEASUREMENT & CONTROL

Article

Transactions of the Institute of Measurement and Control
2018, Vol. 40(13) 3899–3908

DOI: 10.1177/0142331217735050
journals.sagepub.com/home/tim
SAGE

Re-entry guidance for hypersonic vehicle satisfying no-fly zone constraints

Qing Lu and Jun Zhou

Abstract

Re-entry guidance is one of the primary tasks of a global strike mission. Hypersonic and common aero vehicles are currently being investigated for missions like this. This paper proposes a guidance law considering not only the constraints of terminal status and flight process, but also the avoidance of no-fly zones, to meet the requirements of a global strike mission. An improved A* algorithm is proposed first to achieve a real-time trajectory planning process. Then a dynamic optimization guidance law based on the model of a hypersonic vehicle considering single and multiple no-fly zones is founded. Numerical simulations show the robustness and rapidity of this optimization method.

Keywords

Guidance, hypersonic vehicle, no-fly zone, optimal control, re-entry.

Introduction

Global strikes and global persistent attacks are two of the seven United States Air Force Concepts of Operations Actions (Acton and Saalman, 2016). According to these concepts, the USA should have the ability to complete this strike in several minutes or hours. Thus, hypersonic vehicles, which are unmanned aerial vehicles with high speeds, can support this goal. As an important part of current hypersonic vehicle research, re-entry guidance has become a hot and difficult topic.

The guidance methods for hypersonic vehicles may be divided into two categories: methods based on a nominal trajectory and methods using prediction and correction (Guo et al., 2015). Wang and Yan (2013) proposed a high accurate integrated guidance law for re-entry vehicles. Successful tests of shuttles and spacecraft show that the guidance methods above can effectively solve various problems encountered in re-entry (Brunner and Lu, 2008; Lu, 1997, 2008, 2013). In order to complete penetration missions, the avoidance of geographical sensitive areas must be considered. However, little research on this issue has been published. Erzberger and Lee (2015) and Ma et al. (2015) computed optimal turn performance. He et al. (2009), Pan and Ya (2014) and Liu and Zhang (2009) constructed Voronoi diagrams to partition threats. Boyer et al. (2016), Mekala et al. (2016) and Yang and Zhao (2004) specifically addressed intermediate waypoints. Yang and Zhao (2004) used a discrete search strategy. Karimi and Pourtakdoust (2013) and Vian and Moore (2012) used cost to proportion the distance from threats, and Raghunathan et al. (2003) used an interior barrier penalty function technique to avoid no-fly zones. On the basis of the above algorithms, a re-entry trajectory plan method considering no-fly zones and waypoint constraints was proposed by Jorris and Cobb (2009).

The methods above can complete no-fly zone avoidance missions, but some deficiencies should be noticed. For example, the command of the discrete search algorithm from Yang and Zhao will jump when it comes to the search point. Although the method of Erzberger and Lee (2015) is able to avoid no-fly zones, it cannot guarantee the optimality for a given indicator. The method of Ma et al. (2015) can meet various requirements of the aircraft, but it is unable to provide a reasonable approach to handle multiple no-fly zones. Considering the limitations of the methods described above, we establish a complete three-degree-of-freedom (3-DOF) model for hypersonic vehicles. The constraint of the no-fly zone is introduced into the solving process of optimal control based on the 3-DOF model. A bank angle command can be obtained by solving the optimal control problem.

This paper is organized as follows. The complete 3-DOF model is established first. The requirements of the mission are clearly described, and these are completed. An improved A* trajectory planning method is introduced as a reference for following the algorithm. Then a guidance algorithm considering the constraint of the no-fly zone is built to obtain the bank angle command, and the algorithm focused on a single zone is developed to adapt multiple no-fly zones. The new algorithm is compared with the improved A* algorithm. Robustness

Institute of Precision Guidance and Control, Northwestern Polytechnical University, Shaan Xi Xi'an, China

Corresponding author:
Qing Lu, Institute of Precision Guidance and Control, Northwestern Polytechnical University, Postbox 234, 127 Youyi xilu, Shaan Xi Xi'an 710072, China.
Email: lamaxiya1990@163.com

analysis based on a large number of simulations using the proposed algorithm is performed. Lastly, summaries and conclusions are presented. A supplemental proof for the improved A* algorithm and some derivation processes are discussed in the Appendices.

Problem statement

Equations of motion

Hypersonic vehicle flies over a long distance, the impact of earth self-rotation cannot be ignored. We found complete 3-DOF model as follows Zhao (1997):

$$\begin{cases} \dot{V} = -\dfrac{X}{m} - g\sin\theta_T - \omega_e^2 r\left(\cos\phi\sin\phi\cos\sigma_T\cos\theta_T - \cos^2\phi\sin\theta_T\right) \\ \dot{\theta}_T = \dfrac{Y}{mV}\cos\gamma_v - g\dfrac{\cos\theta_T}{V} + \dfrac{V\cos\theta_T}{r} + \dfrac{\omega_e^2 r}{V}\left(\cos\phi\sin\phi\cos\sigma_T\sin\theta_T + \cos^2\phi\cos\theta_T\right) - 2\omega_e\cos\phi\sin\sigma_T \\ \dot{\sigma}_T = -\dfrac{Y}{mV\cos\theta_T}\sin\gamma_v + \dfrac{V\cos\theta_T\sin\sigma_T\tan\phi}{r} - \omega_e^2 r\dfrac{\cos\phi\sin\phi\sin\sigma_T}{V\cos\theta_T} + \dfrac{2\omega_e}{\cos\theta_T}(\cos\sigma_T\sin\theta_T\cos\phi - \sin\phi\cos\theta_T) \\ \dot{\phi} = \dfrac{V\cos\theta_T\cos\sigma_T}{r}, \dot{\lambda} = -\dfrac{V\cos\theta_T\cos\sigma_T}{r\cos\phi}, \dot{r} = V\sin\theta_T \end{cases} \quad (1)$$

where ω_e is the earth self-rotation rate, r is the radial distance from the earth centre to the vehicle, V is the Earth-relative velocity, θ_T is the flight-path angle of the Earth-relative velocity vector, σ_T is the heading angle of the velocity vector, which is measured clockwise in the local horizontal plane from north, γ_v is the bank angle, g is the magnitude of the gravitational acceleration along r, and λ and ϕ are the longitude and latitude. Finally, lift is denoted $Y = C_L S\rho V^2/2$ and drag is denoted $X = C_D S\rho V^2/2$, where ρ is the atmospheric density and S is the reference area. The magnitude of aerodynamic coefficients C_D, C_L is related to the angle of attack, height, Mach number and other factors. The magnitude of the angle of attack is a function of Mach number, which is determined by the terminal state, flight range and control capability of the vehicle. The guidance method below is independent of angle of attack profile. By changing the bank angle, which is the main control parameter of re-entry trajectory, no-fly zones can be effectively avoided.

Terminal state constraints are

$$V_f = V_f^*, \phi_f = \phi_f^*, \lambda_f = \lambda_f^*, r_f = r_f^* \quad (2)$$

where $V_f, \phi_f, \lambda_f, r_f$ are terminal states of velocity, longitude, latitude, the radial distance from the earth centre to the vehicle, and $V_f^*, \phi_f^*, \lambda_f^*, r_f^*$ are the desired terminal states.

The constraints of heat flow, overload, dynamic pressure and equilibrium gliding should also be considered during the flight of the vehicle.

$$\begin{cases} \dot{Q} \le \dot{Q}_{\max}, \sqrt{L^2 + D^2}\Big/ G \le n_{\max} \\ q \le q_{\max}, \left[\dfrac{1}{r} - V^2\right]\left(\dfrac{1}{r}\right) - L\cos\sigma_{EQ} \le 0 \end{cases} \quad (3)$$

where $\dot{Q}_{\max}, n_{\max}, q_{\max}$ are maximum magnitude of heat flow, overload and dynamic pressure, G is the gravity of the vehicle and σ_{EQ} is the flight-path angle of equilibrium gliding. The guidance algorithm solves the problem of finding a suitable command of the bank angle according to current states, to obtain a flight trajectory that satisfies process constraints and terminal constraints.

Mission statement

The overall mission is to make the vehicle fly from a specified initial point to the target and satisfy many constraints at the same time. In order to ensure that the vehicle cannot fly over the no-fly zones, these zones are regarded as a cylindrical area with unlimited height. A no-fly zone is denoted (L, B, R), where L and B are the longitude and latitude of the no-fly zone centre, and R is the radius of the no-fly zone. Information on the initial point, target and no-fly zone are shown in Table 1.

Trajectory planning assumptions

In order to solve the problem above, some important assumptions should be made.

1) Only consider gravity along the direction from the earth centre to the vehicle.
2) No-fly zones are regarded as circular areas with specific radius. They may be denoted (ϕ_w, λ_w, R_w), where ϕ_w is the longitude, λ_w is the longitude and R_w is the radius of the no-fly zone.
3) The vehicle must not enter the no-fly zone.
4) The coordinates of the target are specified.
5) Angle of attack and bank angle are two control parameters that are restricted.
6) Angle of attack profile is predetermined as a function of Mach number.
7) The heat flow of the stagnation point is restricted

Table 1. Information about specified point.

Descriptor	Initial	Target	No-fly zone
Longitude (°)	153	−100 (260)	−150 (210)
Latitude (°)	58	35	55

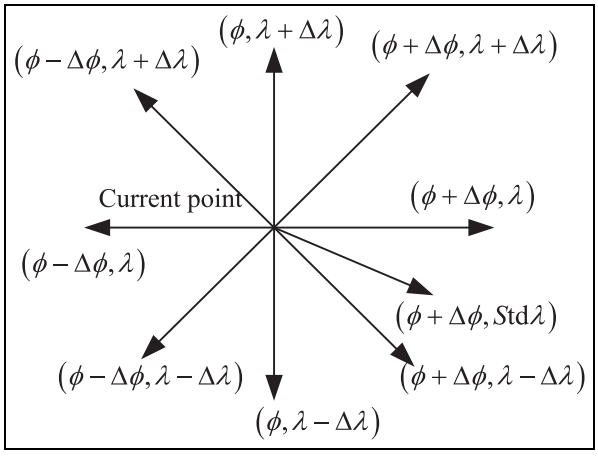

Figure 1. Extended flight points.

Methodology

The main object of the method is to design a guidance law to make the vehicle fly from the current point to the target and fulfil various constraints at the same time. The angle of attack, which can affect the height of the vehicle, may be designed as a function of Mach number. More attention is paid to bank angle, that is, the lateral manoeuvring of the vehicle. An improved A* algorithm is applied to plan the trajectory at first, and then a guidance method, which is based on the trajectory, may be obtained. Finally, a dynamic optimization algorithm is introduced to complete the no-fly zone avoidance mission.

Improved A algorithm*

The introduction of cost function. The longitudinal design of the vehicle is predetermined by the angle of attack to ensure that all flight points are reachable. As a result, there is no need to consider the inspired item related to the target in the cost function. Distance cost and expense cost are included as items of the cost function as follows (Szczerba et al., 2000).

$$f = w_1 S + w_2 L \tag{4}$$

where S denotes the total range from the current point to the target and L is the nearest distance from the trajectory to no-fly zone. Variable weights are used here; weights are computed by using $\omega_2 = R/L$ and $\omega_1 = 1 - \omega_2$, where R represents the radius of the no-fly zone.

Trajectory generation. Latitude and longitude of the starting point are ϕ_0 and λ_0, latitude and longitude of the target are ϕ_f and λ_f, latitude and longitude of current point are ϕ and λ, and current cumulative latitude and longitude are $\Delta\phi$ and $\Delta\lambda$. The search process comes to an end when the distance between the current point and the target is less than ε.

1) Initial judgment: If the initial point or the target is in the no-fly zones, end the search process. No trajectory is obtained.
2) Generation of flight point: a) The current point is (ϕ, λ). Considering the theory of the A* algorithm, eight flight points of all directions are $(\phi + \Delta\phi, \lambda + \Delta\lambda)$, $(\phi + \Delta\phi, \lambda)$, $(\phi + \Delta\phi, \lambda - \Delta\lambda)$, $(\phi, \lambda - \Delta\lambda)$, $(\phi, \lambda + \Delta\lambda)$, $(\phi - \Delta\phi, \lambda + \Delta\lambda)$, $(\phi - \Delta\phi, \lambda)$ and $(\phi - \Delta\phi, \lambda - \Delta\lambda)$. These are points to be extended and are put into the OPEN table. In order to ensure that the flight point can reach the target as soon as possible, a reference point $(\phi + \Delta\phi, S\text{td}\lambda)$ towards the target is added, where $S\text{td}B$ represents standard longitude of the circular arc towards the target. This point should also be put into the OPEN table. The positions of the points above are shown in Figure 1.
b) The nine points above are used to extend the CLOSE table. Delete the point to be extended, which is in no-fly zone. Choose the best one in the remaining points by using the cost function and put it into the CLOSE table.
3) End condition:

$$Stogo < \varepsilon \tag{5}$$

where ε is a constant. The search process comes to an end when the distance between the current point and the target is less than ε. The target is added to the CLOSE table.
4) Smoothing process: The trajectory obtained from above method is constructed by lines between flight points. As a result, it is not smooth enough. In order to make the trajectory more feasible, there is a need to make it smooth. The trajectory may be denoted

$$\mathbf{ROAD} = (Point_0, Point_1, Point_2, \cdots, Point_n) \tag{6}$$

where $Point_0, Point_1, Point_2, \cdots, Point_n$ are flight points. Selecting two points from the trajectory arbitrarily, delete the points between these two points if the line between them is not in the no-fly zone. Repeating the operation from the start point, a smoothing optimal trajectory may be finally obtained. The remaining flight points are:

$$\mathbf{ROAD}' = (Point'_0, Point'_1, Point'_2, \cdots, Point'_k) \tag{7}$$

5) A nominal trajectory may be obtained from the above points. The convergence of the algorithm will be proved in Appendix 1. Based on the improved A* algorithm above, a feasible nominal trajectory may be obtained. However, the trajectory is derived without considering the specific dynamic model of the vehicle. As a result, it will be difficult to put this algorithm into practice. In order to solve the problem, a dynamic optimization method is introduced to obtain optimal guidance command.

Algorithm for single no-fly zone

The problem of dynamic optimization can be described as choosing a cost function and finding the optimal solution under the constraints of dynamic equations, control inequalities, middle states and so on.

Optimal model. A suitable cost function is needed in order to found optimal model (Liao et al., 2015).

$$J = \Phi\left[x(t_f), t_f\right] + \int_{t_0}^{t_f} F[x(t), u(t), t]dt \tag{8}$$

where $\Phi\left[x(t_f), t_f\right]$ is the terminal constraint and $F[x(t), u(t), t]$ is the integrand function. The constraint of terminal position may be denoted

$$\mathbf{P}(x(t_f), t_f) = \begin{bmatrix} \phi(t_f) - \phi_f \\ \lambda(t_f) - \lambda_f \end{bmatrix} = 0 \tag{9}$$

where $(\phi(t_f), \lambda(t_f))$ is the coordinate of latitude and longitude at terminal time, and (ϕ_f, λ_f) is the coordinate of the target. Considering the constraint of the no-fly zone, the inequality constraint is introduced:

$$g\left[x(t_f), t_f\right] = S_w - R_w > 0 \tag{10}$$

where S_w is the length of the earth arc from the current point to the centre of the no-fly zone and R_w is the radius of the no-fly zone. The constraint of inequality may be converted to the constraint of the equation.

$$W = S_w - R_w - \alpha^2 = 0 \quad \alpha \neq 0 \tag{11}$$

where α is a constant, which is not equal to zero. We pay more attention to the constraints of the no-fly zone and terminal state, so we set $F[x(t), u(t), t] = 0$.

After all the constraints are determined, they are put together with dynamic equations by using multipliers. Terminal states, which are used to determine the terminal magnitude of the costates, are not included in the Hamiltonian. Thus, the Hamiltonian is

$$H_x = \bar{\lambda}^T \boldsymbol{f} + \mu_w W \tag{12}$$

where $\bar{\lambda}$ are the costates and μ_w is a coefficient related to the no-fly zone. When the no-fly zone is considered, $\mu_w \neq 0$; otherwise $\mu_w = 0$. $\boldsymbol{f} = \dot{\boldsymbol{x}} = \left[\dot{V}, \dot{\theta}_T, \dot{\sigma}_T, \dot{\phi}, \dot{\lambda}, \dot{r}\right]$ are dynamic equations.

The case for $\mu_w = 0$. The impact of the no-fly zone can be neglected when the vehicle is far from it. Then a common optimal control method may be applied to obtain a guidance command. Combining with the 3-DOF equation and optimal model, the costates equations may be obtained.

$$\dot{\bar{\lambda}} = -\frac{\partial H}{\partial x} \tag{13}$$

For Equation (1), we have $\frac{\partial Y}{\partial V} = C_L S\rho V$, $\frac{\partial X}{\partial V} = C_x S\rho V$. Costate equations may be obtained based on Equations (1), (12) and (13).

$$\dot{\bar{\lambda}}_1 = -\frac{\partial H}{\partial V} = -\left[-\bar{\lambda}_1 \frac{C_D S\rho V}{m} + \bar{\lambda}_2\left(\frac{C_L S\rho \cos\gamma_v}{2m} + g\frac{\cos\theta_T}{V^2} + \frac{\cos\theta_T}{r}\right) + \bar{\lambda}_3\left(-\frac{C_L S\rho \sin\gamma_v}{2m\cos\theta_T} + \frac{\cos\theta_T \sin\sigma_T \tan\phi}{r}\right) + \bar{\lambda}_4 \frac{\cos\theta_T \cos\sigma_T}{r} - \bar{\lambda}_5 \frac{\cos\theta_T \cos\sigma_T}{r\cos\phi} + \bar{\lambda}_6 \sin\theta_T\right]$$

$$\dot{\bar{\lambda}}_2 = -\frac{\partial H}{\partial \theta_T} = -\left[\bar{\lambda}_1\left(-\sin\theta_T + \omega_e^2 r(\cos\phi \sin\phi \cos\sigma_T \sin\theta_T + \cos^2\phi \cos\theta_T)\right) + \bar{\lambda}_2\left(g\frac{\cos\theta_T}{V} - \frac{V\sin\theta_T}{r} + \frac{\omega_e^2 r}{V}(\cos\phi \sin\phi \cos\sigma_T \cos\theta_T - \cos^2\phi \sin\theta_T)\right) + \bar{\lambda}_3\left(-\frac{Y\sin\theta_T \sin\gamma_v}{mV\cos^2\theta_T} + \omega_e^2 r\frac{\cos\phi \sin\phi \sin\sigma_T \sin\theta_T}{V\cos^2\theta_T} + \frac{2\omega_e}{\cos\theta_T}(\cos\sigma_T \cos\theta_T \cos\phi + \sin\phi \sin\theta_T)\right) - \bar{\lambda}_4 \frac{V\sin\theta_T \cos\sigma_T}{r} - \bar{\lambda}_5 \frac{V\sin\theta_T \cos\sigma_T}{r\cos\phi} + \bar{\lambda}_6 V\cos\theta_T\right]$$

$$\dot{\bar{\lambda}}_3 = -\frac{\partial H}{\partial \sigma_T} = -\left[\bar{\lambda}_1 \omega_e^2 r(\cos\phi \sin\phi \sin\sigma_T \cos\theta_T) + \bar{\lambda}_2\left(-\frac{\omega_e^2 r}{V}\cos\phi \sin\phi \cos\sigma_T \sin\theta_T - 2\omega_e \cos\phi \cos\sigma_T\right) + \bar{\lambda}_3\left(\frac{V\cos\theta_T \cos\sigma_T \tan\phi}{r} - \omega_e^2 r\frac{\cos\phi \sin\phi \cos\sigma_T}{V\cos\theta_T} - \frac{2\omega_e}{\cos\theta_T}\sin\sigma_T \sin\theta_T \cos\phi\right) - \bar{\lambda}_4 \frac{V\cos\theta_T \sin\sigma_T}{r} + \bar{\lambda}_5 \frac{V\cos\theta_T \sin\sigma_T}{r\cos\phi}\right]$$

$$\dot{\bar{\lambda}}_4 = -\frac{\partial H}{\partial \phi} = -\left[-\bar{\lambda}_1 \omega_e^2 r(\cos^2\phi \cos\sigma_T \cos\theta_T - \sin^2\phi \cos\sigma_T \cos\theta_T + 2\sin\phi \cos\phi \sin\theta_T) + \bar{\lambda}_2\left(\frac{\omega_e^2 r}{V}(\cos^2\phi \cos\sigma_T \sin\theta_T - \sin^2\phi \cos\sigma_T \sin\theta_T - 2\sin\phi \cos\phi \cos\theta_T) + 2\omega_e \sin\phi \sin\sigma_T\right) + \bar{\lambda}_3\left(\frac{V\cos\theta_T \sin\sigma_T}{r\cos^2\phi} + \omega_e^2 r\frac{\sin^2\phi \sin\sigma_T}{V\cos\theta_T} - \omega_e^2 r\frac{\cos^2\phi \sin\sigma_T}{V\cos\theta_T} - \frac{2\omega_e}{\cos\theta_T}\cos\sigma_T \sin\theta_T \sin\phi - \frac{2\omega_e}{\cos\theta_T}\cos\phi \cos\theta_T\right) - \bar{\lambda}_5 \frac{V\cos\theta_T \cos\sigma_T \sin\phi}{r\cos^2\phi}\right]$$

$$\dot{\bar{\lambda}}_5 = -\frac{\partial H}{\partial \lambda} = 0$$

$$\begin{aligned}\dot{\bar{\lambda}}_6 = -\frac{\partial H}{\partial r} = &-\left[-\bar{\lambda}_1\omega_e^2\left(\cos\phi\sin\phi\cos\sigma_T\cos\theta_T - \cos^2\phi\sin\theta_T\right)\right.\\ &+\bar{\lambda}_2\left(-\frac{V\cos\theta_T}{r^2} + \frac{\omega_e^2 r}{V}\left(\cos\phi\sin\phi\cos\sigma_T\sin\theta_T + \cos^2\phi\cos\theta_T\right)\right)\\ &\left.+\bar{\lambda}_3\left(-\frac{V\cos\theta_T\sin\sigma_T\tan\phi}{r^2} - \omega_e^2\frac{\cos\phi\sin\phi\sin\sigma_T}{V\cos\theta_T}\right)\right]\\ &-\bar{\lambda}_4\frac{V\cos\theta_T\cos\sigma_T}{r^2} + \bar{\lambda}_5\frac{V\cos\theta_T\cos\sigma_T}{r^2\cos\phi}\end{aligned} \tag{14}$$

According to the theory of optimal control, γ_v is chosen as the control valuable. The optimal control equation should be solved:

$$\frac{\partial H}{\partial u} = \frac{\partial H}{\partial \gamma_v} = -\bar{\lambda}_2\frac{Y\sin\gamma_v}{mV} - \bar{\lambda}_3\frac{Y\cos\gamma_v}{mV\cos\theta_T} = 0 \tag{15}$$

and that equation rearranged:

$$\tan\gamma_v = -\frac{\bar{\lambda}_3}{\bar{\lambda}_2\cos\theta_T} \Rightarrow \gamma_v = -\arctan\frac{\bar{\lambda}_3}{\bar{\lambda}_2\cos\theta_T} \tag{16}$$

The control command above is used when $\mu_w = 0$. The initial values of the costates are determined by the terminal states. The optimal command should be divided into two parts: the first is before the no-fly zone and the second is after the no-fly zone. Complete the trajectory planning process by choosing a trajectory that can fulfil the constraint of the terminal states.

The handling of no-fly circle

For the case of a no-fly circle, the vehicle should fly along the border of the no-fly circle and ensure that the vehicle does not enter the no-fly zone. Assume that the no-fly zone is larger than the minimum turn radius, so that the vehicle can fly along the border of the no-fly zone. That is to say we have $W = 0$ in Equation (11). No command jump requires that $W^{(1)} = 0$. In order to obtain the command of the bank angle we should also have $W^{(2)} = 0$.

$$\boldsymbol{U} = \begin{bmatrix} W \\ W^{(1)} \\ W^{(2)} \end{bmatrix} = 0 \tag{17}$$

We consider the sphere model here and use the formula for the earth arc.

$$\begin{gathered} C = \sin\phi\sin\phi_w\cos(\lambda - \lambda_w) + \cos\phi\cos\phi_w \\ S_w = R\arccos(C) \end{gathered} \tag{18}$$

where C is a intermediate variable and $R = 6371000$ is the radius of the earth. East longitude takes a positive value and west longitude takes a negative value. North latitude takes $\left(90^\circ - \lambda\right)$ and south latitude takes $\left(90^\circ + \lambda\right)$. S_w is the length from the current position to the centre of the no-fly zone. Substituting Equation (11) into Equation (17) produces

$$\begin{bmatrix} S_w - R_w - \alpha^2 \\ S_w^{(1)} \\ S_w^{(2)} \end{bmatrix} = 0 \tag{19}$$

Compute the time derivatives of C and S_w

$$\begin{aligned} \frac{\partial C}{\partial t} = &\cos\phi\sin\phi_w\cos(\lambda - \lambda_w)\dot{\phi} - \sin\phi\sin\phi_w \\ &\sin(\lambda - \lambda_w)\dot{\lambda} - \sin\phi\cos\phi_w\dot{\phi} \\ S_w^{(1)} = &R\frac{-1}{\sqrt{1-C^2}}\frac{\partial C}{\partial t} = 0 \end{aligned} \tag{20}$$

Combining with $\dot{\phi} = \frac{V\cos\theta_T\cos\sigma_T}{r}$ and $\dot{\lambda} = -\frac{V\cos\theta_T\cos\sigma_T}{r\cos\phi}$ in Equation (1), the expression of $S_w^{(1)}$ can be obtained. For Equation (20) we have $R \neq 0$, $\frac{-1}{\sqrt{1-C^2}} \neq 0$, so $\frac{\partial C}{\partial t} = 0$. The command of the bank angle may be obtained from $S_w^{(2)} = 0$. The solving process, which is quite complex, is given in Appendix 2. Here we give the expression of the bank angle directly.

$$\gamma_v = -2 * \arctan\left(\left(N_6 + \sqrt{-M_3^2 + N_5^2 + N_6^2}\right)\Big/\left(M_3 - N_5\right)\right) \tag{21}$$

where M_3, N_5, N_6 are all polynomials and are explained in Appendix 2. The vehicle can fly along the border of the no-fly circle when Equation (21) is used.

Command transfer

The entire process of re-entry can be divided into three segments according to the value of μ_w; they are the initial phase, the no-fly zone phase and the target phase. The boundary conditions at the end of each segment must be satisfied. That is to say no command jump in the costates or Hamiltonian is allowed. t^- represents the final time of the previous segment and t^+ represents the initial time of the next segment. Costates and Hamiltonian must be continuous. The jump conditions of them can be shown as follows (Jorris and Cobb, 2008, 2009)

$$\lambda(t^-) = \lambda\left(t^+\right) + \boldsymbol{K}_U^T\partial\boldsymbol{U}/\partial\boldsymbol{x}, H(t^-) = H\left(t^+\right) + \boldsymbol{K}_U^T\partial\boldsymbol{U}/\partial t \tag{22}$$

where $\boldsymbol{K}_U^T$ is the vector of six multipliers. The vector may be different for each jump, but the form of the equations remains the same. t can be changed so that Equation (22) can be generalized to apply to any one of the jumps. According to the continuity requirement of the costates and Hamiltonian, $\dot{\boldsymbol{\lambda}}(t) = 0, \dot{H}(t) = 0$ may be obtained. $\dot{\boldsymbol{\lambda}}(t) = 0, \dot{H}(t) = 0$ leads to the following:

$$\boldsymbol{\lambda}(t^-) = \boldsymbol{\lambda}\left(t^+\right), H(t^-) = H\left(t^+\right) \tag{23}$$

Combining with the partial derivatives of $\mathbf{U}$, constant vector $\boldsymbol{K}_U^T$ can be solved.

If the radius of the no-fly zone is larger than minimum turn radius, the vehicle begins a turning manoeuvre along the border of the no-fly zone; otherwise, the vehicle begins a

turning manoeuvre along the circle of minimum turn radius. The initial value of costates should be adjusted to ensure that the vehicle can reach the target and complete the whole process of guidance.

Algorithm for multiple no-fly zones

The algorithm for multiple no-fly zones is based on the method for a single zone. It should be emphasized here that the velocity hypersonic vehicle is very high. As a result, the manoeuvrability of the vehicle is limited. Some assumptions about the arrangement of no-fly zones must be emphasized here.

Assumption 1. If some no-fly circles coincide, we can replace them by a large one.

Assumption 2. No-fly zones that have no impact on the trajectory are not considered here.

The algorithm is made based on the assumptions above. We pay more attention to the trajectory between the two no-fly zones. The vehicle flies along the border of the no-fly zone or minimum turn radius to perform the turning manoeuvre. When the flight direction of the vehicle and the next no-fly zone are at a tangent, the vehicle should fly along the current direction. After reaching the next no-fly circle, the vehicle flies along the border of the circle. The guidance command between the no-fly zones can be obtained by repeating the above process, as shown in Figure 2, where A is the current position of the vehicle, V is the velocity, O_{w1} and O_{w2} are centres of two no-fly zone, R_{w1} and R_{w2} are radius of the two no-fly zones.

The command of the bank angle between the two no-fly zones can be obtained by using the theory of optimal control. Command jumps can be handled by the method for a single no-fly zone. Adjustment of the initial value of costates ensures that the vehicle may reach the target.

Simulations and analysis

In order to prove the practicality of the guidance algorithm in this paper, a kind of hypersonic vehicle is chosen as a research object for simulations. For the problem proposed in this paper, the initial flight direction must point to the target and there is no constraint on terminal flight direction.

Compare with A* algorithm

Information on initial point, target and no-fly zone is shown in Table 1. The radius of the no-fly zone is 1200 km. The vehicle flies from the current point to the target while avoiding the no-fly zone at the same time. The integrand function is chosen as $F[x(t), u(t), t] = t$ to minimize the flight time.

Both the optimal guidance method and improved A* algorithm may find a trajectory that can reach the target, but their shapes are quite different. The trajectory produced by the optimal guidance method is smoother. Figure 4 can be obtained by partially enlarging Figure 3. It may be seen from the figure that the initial flight direction of the optimal guidance method points to the target. On the other hand, after the smoothing process, the trajectory obtained by the A* algorithm is smooth enough but as the trajectory planning process is not combined with actual flight states, there is a

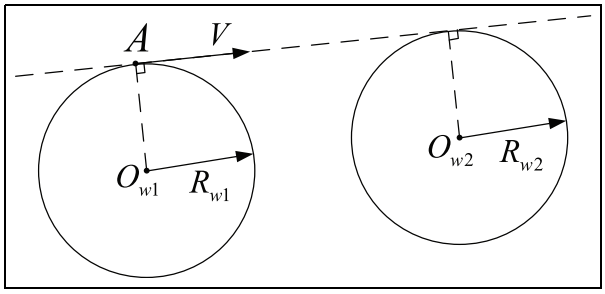

Figure 2. Schematic for switching between no-fly zones.

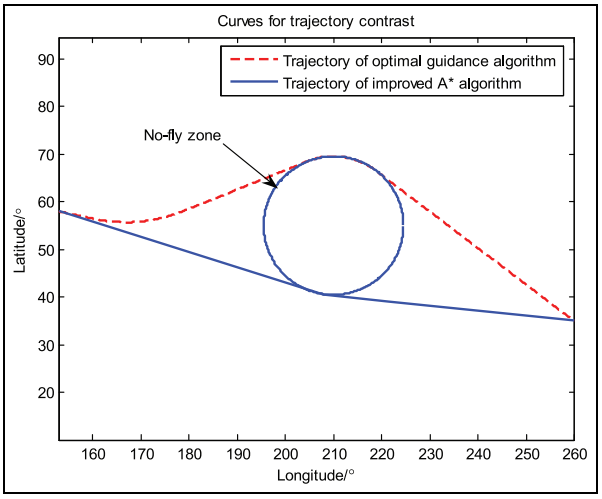

Figure 3. Comparison of trajectories.

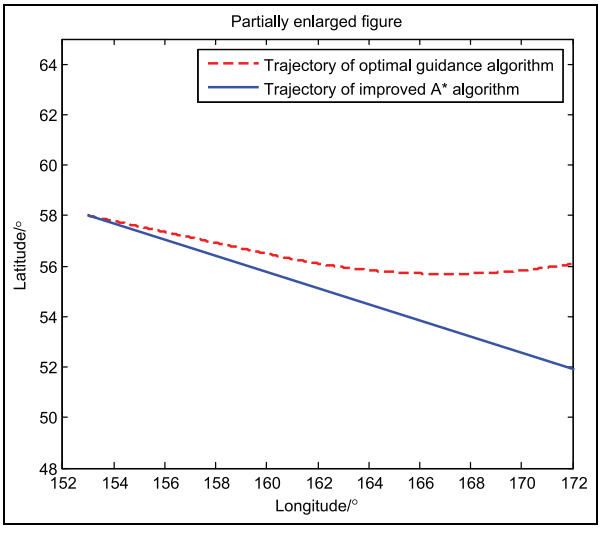

Figure 4. Partially enlarged figure.

Table 2. Simulations for different targets.

Targets	States		
	Longitude (°)	Latitude (°)	Time for convergence
Target 1	−100 (260)	35	0.60
Target 2	−110 (250)	50	0.59
Target 3	−120 (240)	45	0.57
Target 4	−100 (260)	60	0.63

Table 3. Simulations for different no-fly zones.

No-fly zone	States	
	Longitude (°)	Latitude (°)
No-fly zone 1	−150 (210)	55
No-fly zone 2	−160 (200)	45
No-fly zone 3	−120 (240)	40

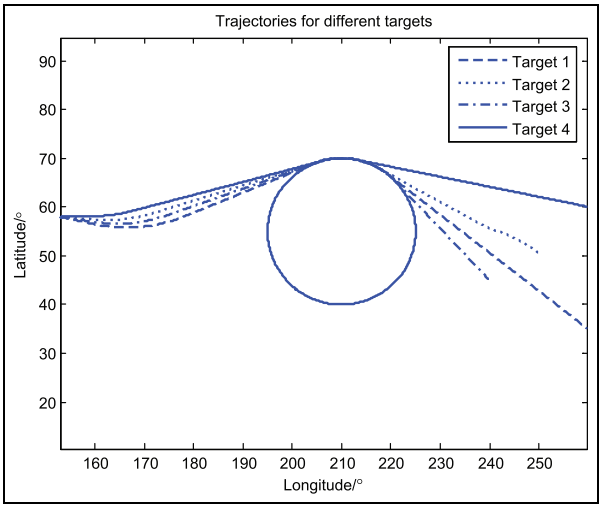

Figure 5. Adaptability of different targets.

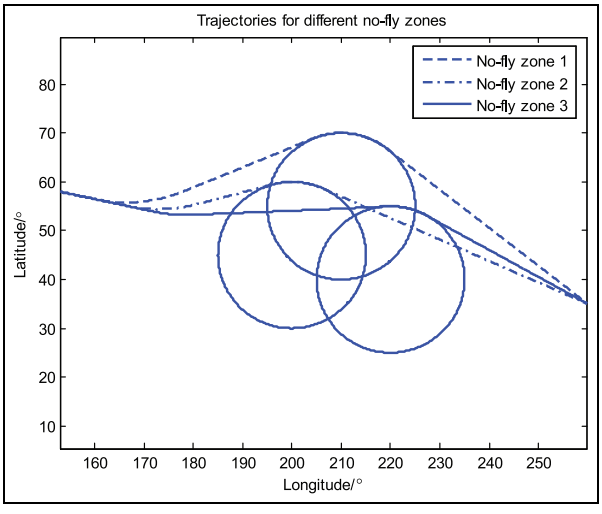

Figure 6. Trajectory planning for different no-fly zones.

quite significant deviation from the initial launch direction. The deviation in trajectory will result in a jump of the guidance command, which will make it very difficult to track the trajectory. This situation also exists at the junction of the straight trajectory and the turning section. Besides, the A* algorithm can only give position information on the trajectory instead of the guidance command. On the other hand, the optimal re-entry guidance method successfully solves the problem of the command jump at junctions. In other words, the optimal re-entry guidance method, which consider the change of command at junctions, is more practical than the A* algorithm.

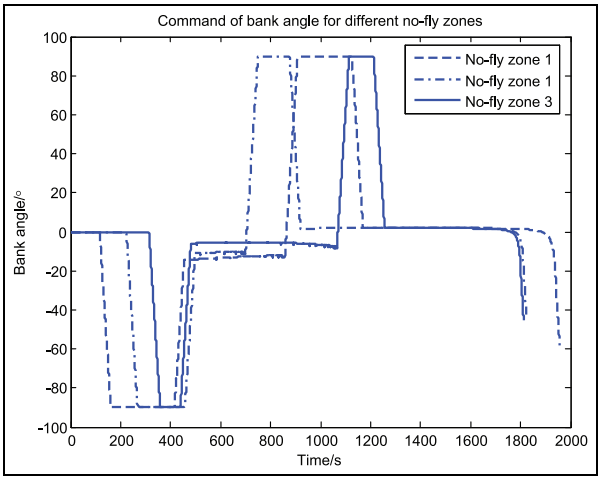

Figure 7. Command of bank angle for different no-fly zones.

Adaptability analysis

Due to the high speed of hypersonic vehicles, guidance algorithms should converge in very short time. Different targets are chosen for simulations and convergence time will be recorded. The simulations are conducted on an ordinary desktop computer. Information on different targets is shown in Table 2.

It may be seen from Figure 5 that the optimal guidance algorithm proposed by this paper can produce reasonable trajectories for different targets and the convergent time is within 1 s. In order to validate further the adaptability of the algorithm, we chose different no-fly zones for simulations. Here we chose target 1 as shown in Table 2 and the information on the no-fly zones is shown in Table 3; the radius of the no-fly zones is 1200 km.

It may be seen from Figures 6 and 7 that the algorithm proposed by this paper can also adapt different no-fly zones and quickly produce trajectories pointing to the target. The

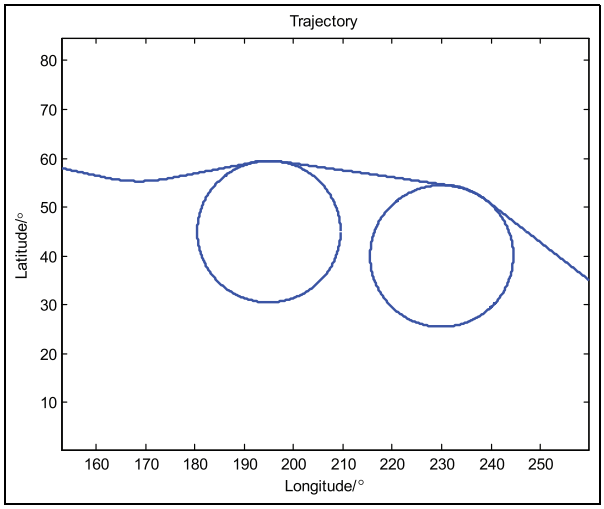

Figure 8. Simulation for two no-fly zones.

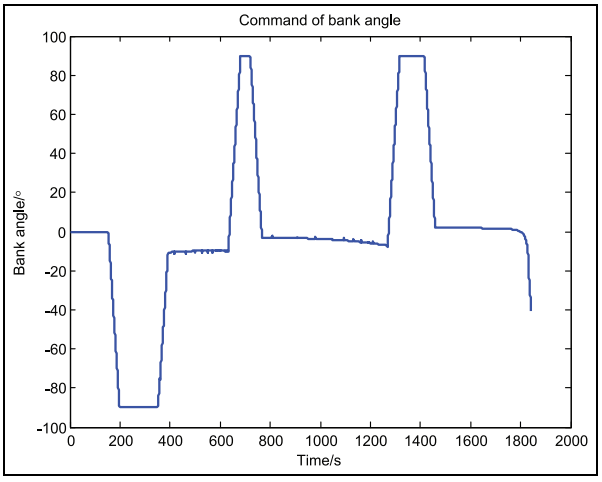

Figure 9. Command of bank angle for two no-fly zones.

command of the bank angle corresponds with the trajectory and has no jump. Terminal divergence is due to the situation in which the vehicle is too close to the target. Simulation results for two no-fly zones are given as follows. The situation for more no-fly zones is the same.

It can be seen from Figures 8 and 9 that the guidance algorithm of this paper can produce a reasonable trajectory for a situation of multiple no-fly zones and completes the mission. Furthermore, there is no command jump.

Conclusion

The simulation results and derivations above shows that the guidance law proposed in this paper can fulfil the requirements of fast trajectory planning for a hypersonic vehicle. The improved A* algorithm that gives a rough shape of the trajectory is proposed as a reference for the optimal guidance algorithm. Furthermore, it also provides a comparison for the algorithm of this paper. By choosing a suitable cost function, the algorithm in this paper can achieve optimal performance for the index concerned. At the same time, the algorithm fully considers the command at junctions to make the change of command smoother. Many kinds of simulations verify the robustness of this method under the condition of various targets, various no-fly zones and multiple no-fly zones. The command of the bank angle given by this method can satisfy tracking requirements of the control system. However, there are still some deficiencies. For example, there are some limitations when we chose flight time as a performance index, which cannot illustrate the effect of other factors upon the re-entry guidance for hypersonic vehicle. Under these circumstances, future work will focus on the effect of different performance indexes on the optimal guidance method.

Declaration of conflicting interest

The author(s) declared no potential conflicts of interest with respect to the research, authorship, and/or publication of this article.

Funding

The author(s) received no financial support for the research, authorship, and/or publication of this article.

References

Acton JM and Saalman L (2016) Conventional prompt global strike and strategic stability. *Limnology & Oceanography* 56(6): 2251–2264.

Boyer J, Auletto R and Baloche N (2016) Method of adapting a segment of an aircraft trajectory with constant ground gradient segment according to at least one performance criterion. US20160085239.

Brunner CW and Lu P (2012) Skip entry trajectory planning and guidance. *Journal of Guidance Control & Dynamics* 31(5): 1210–1219.

Erzberger H and Lee HQ (2015) Optimum horizontal guidance techniques for aircraft. *Journal of Aircraft* 8(2): pp. 95–101.

Guo J, Wu X and Tang S (2015) Autonomous gliding entry guidance with geographic constraints. *Chinese Journal of Aeronautics* 28(5): 1343–1354.

He YP, Zhang A and Liu H (2009) Path planning for UCAV based on Voronoi diagram and ant colony optimization. *Electronics Optics & Control* 16(11): 22–24.

Jorris TR and Cobb RG (2008) Multiple method 2-D trajectory optimization satisfying waypoints and no-fly zone constraints. *Journal of Guidance, Control and Dynamics* 31(3): 543–553.

Jorris TR and Cobb RG (2009) Three-dimensional trajectory optimization satisfying waypoint and no-fly zone constraints. *Journal of Guidance Control and Dynamics* 32(2): 551–572.

Karimi J and Pourtakdoust SH (2013) Optimal maneuver-based motion planning over terrain and threats using a dynamic hybrid PSO algorithm. *Aerospace Science & Technology* 26(1): 60–71.

Liao F, Ji H and Xie Y (2015) A nearly optimal control for spacecraft rendezvous with constrained controls. *Transactions of the Institute of Measurement & Control*, 38(7): 832–845.

Liu L and Zhang S (2009) Voronoi diagram and GIS-based 3D path planning. In: *International Conference on Geoinformatics*. Washington, DC: IEEE, pp. 1–5.

Lu P (1997) Entry guidance and trajectory control for reusable launch vehicle. *Journal of Guidance, Control, and Dynamics* 20(1): 143–149.

Lu P (2008) Predictor-corrector entry guidance for low lifting vehicles. *Journal of Guidance, Control, and Dynamics* 31(4): 1067–1075.

Lu P (2013) Gliding guidance of high L/D hypersonic vehicles. In: *Guidance, Navigation, and Control and Co-located Conferences*, 19–22 August, Boston, MA.

Mekala AR, Madria S and Linderman M (2016) Aerial vehicle trajectory design for spatio-temporal task aggregation. In: *International Conference on Unmanned Aircraft Systems*. Washington, DC: IEEE, pp. 1085–1094.

Ma DM, Shiau JK, Su YJ, et al. (2015) Optimal level turn of solar-powered unmanned aerial vehicle flying in atmosphere. *Journal of Guidance Control & Dynamics* 33(5): 1347–1356.

Pan GZ and Ya-N LI (2014) Route planning for UAVs based on improved Voronoi diagram. *Electronics Optics & Control* 2014-04.

Raghunathan AU, Gopal V, Subramanian D, et al. (2003) 3D conflict resolution of multiple aircraft via dynamic optimization. In: *AIAA Guidance, Navigation, and Control Conference and Exhibit*, AIAA, Reston, VA, 11–14 August.

Szczerba RJ, Galkowski P, Glickstein IS, et al. (2000) Robust algorithm for real-time route planning. *IEEE Transactions on Aerospace and Electronic Systems* 36(3): 869–878.

Vian JL and Moore JR (2012) Trajectory optimization with risk minimization for military aircraft. *Journal of Guidance Control & Dynamics* 12(3): 311–317.

Wang ZG and Yan S (2013) Research on high accuracy guidance law for reentry vehicles. *Applied Mechanics & Materials* 427–429: 81–84.

Yang H and Zhao YJ (2004) Efficient trajectory synthesis through specified waypoints. In: *AIAA 3rd 'Unmanned Unlimited' Technical Conference*, AIAA, Reston, VA, 20–23 September.

Zhao HY (1997) *Reentry guidance and dynamics of aircraft*. Changsha: National University of Defense Technology Press.

Appendices

Appendix 1: Proof of convergence of improved A* algorithm

The convergence of the trajectory refers to the concept that the trajectory may always reach the target for any initial point. In other words, the vehicle should always fly towards the target during the search process. In order to complete the proof, some assumptions are necessary.

Assumption A1. The search space for improved A* algorithm is bounded. This assumption ensures that the search process will not last forever.

Assumption A2. There always exists a feasible trajectory between any two points to be extended.

The feasibility of the search algorithm may be ensured by A2.

We consider the distance between current point and the target, which may be defined as *Stogo*. In the same way, the distance between the next point and the target may be defined as $Stogo_{next}$. According to A1, there always exists a feasible trajectory between the current point and the next point. So the following equation may be obtained based on the definitions above.

$$\Delta S = Stogo - Stogo_{next} \tag{24}$$

where ΔS is a variable that may be negative or positive.

When ΔS is positive, which means *Stogo* is larger than $Stogo_{next}$, we may draw the conclusion that the next point is closer to the target than current point. So the vehicle is flying towards the target, which fulfils the convergence requirement. On the other hand, when ΔS is negative, this means *Stogo* is smaller than $Stogo_{next}$. The vehicle is flying away from the target in order to avoid the no-fly zones. According to the principle $\omega_2 = R/L$ and $\omega_1 = 1 - \omega_2$, the value of L will increase, and as a result the value of ω_1 will keep increasing during the following search process until the next point makes the vehicle flying towards the target. In other words, we may draw the conclusion that whether ΔS is positive or negative, the convergence requirement can always be fulfilled. When the searching process reaches the target, a suitable ε should be chosen to ensure that the terminal ending condition can be satisfied and the flight point can reach the target.

Appendix 2: Solving process of $S_w^{(2)} = 0$

A detail derivation for the command of the bank angle for a single no-fly circle is given in this section.

From (20) we have

$$S_w^{(2)} = -R\left(1 - C^2\right)^{-\frac{3}{2}} C \frac{\partial C}{\partial t}\frac{\partial C}{\partial t} - R\frac{1}{\sqrt{1 - C^2}} C^{(2)} \tag{25}$$

where $\frac{\partial C}{\partial t} = 0$. Then we may obtain

$$S_w^{(2)} = -R\frac{1}{\sqrt{1 - C^2}} C^{(2)} \tag{26}$$

Combining with (20) and computing the second derivative of C:

$$\begin{aligned} C^{(2)} = & -\sin\phi\sin\phi_w\cos(\lambda - \lambda_w)\dot{\phi}\dot{\phi} - \cos\phi\sin\phi_w \\ & \sin(\lambda - \lambda_w)\dot{\phi}\dot{\lambda} - \cos\phi\sin\phi_w\sin(\lambda - \lambda_w)\dot{\lambda}\dot{\phi} - \sin\phi \\ & \sin\phi_w\cos(\lambda - \lambda_w)\dot{\lambda}\dot{\lambda} - \cos\phi\cos\phi_w\dot{\phi}\dot{\phi} + \cos\phi \\ & \sin\phi_w\cos(\lambda - \lambda_w)\ddot{\phi} - \sin\phi\sin\phi_w \\ & \sin(\lambda - \lambda_w)\ddot{\lambda} - \sin\phi\cos\phi_w\ddot{\phi} \end{aligned} \tag{27}$$

According to dynamic equations $\dot{\phi} = \frac{V\cos\theta_T\cos\sigma_T}{r}$ and $\dot{\lambda} = -\frac{V\cos\theta_T\cos\sigma_T}{r\cos\phi}$, the first five parts of $C^{(2)}$ are independent of bank angle. They may be written as

$$\begin{aligned} M_1 = & -\sin\phi\sin\phi_w\cos(\lambda - \lambda_w)\dot{\phi}\dot{\phi} - \cos\phi\sin\phi_w\sin(\lambda - \lambda_w)\dot{\phi}\dot{\lambda} \\ & -\cos\phi\cos\phi_w\dot{\phi}\dot{\phi} + \cos\phi\sin\phi_w\cos(\lambda - \lambda_w)\ddot{\phi} - \cos\phi\cos\phi_w\dot{\phi}\dot{\phi} \end{aligned}$$

The variables before $\ddot{\phi}$ and $\ddot{\lambda}$ in (27) can be regarded as coefficients and written as

$$N_1 = \cos\phi\sin\phi_w\cos(\lambda - \lambda_w) - \sin\phi\cos\phi_w,$$

$$N_2 = -\sin\phi\sin\phi_w\sin(\lambda - \lambda_w)$$

As a result, we have

$$C^{(2)} = M_1 + N_1\ddot{\phi} + N_2\ddot{\lambda} \tag{28}$$

Performing the second derivation of $\ddot{\phi}$ and $\ddot{\lambda}$:

$$\ddot{\phi} = \frac{\cos\theta_T\cos\sigma_T}{r}\dot{V} - \frac{V\sin\theta_T\cos\sigma_T}{r}\dot{\theta}_T - \frac{V\cos\theta_T\sin\sigma_T}{r}\dot{\sigma}_T - \frac{V\cos\theta_T\cos\sigma_T}{r^2}\dot{r}$$

$$\ddot{\lambda} = -\frac{\cos\theta_T\cos\sigma_T}{r\cos\phi}\dot{V} + \frac{V\sin\theta_T\cos\sigma_T}{r\cos\phi}\dot{\theta}_T + \frac{V\cos\theta_T\cos\sigma_T}{r\cos\phi}\dot{\sigma}_T - \frac{V\cos\theta_T\cos\sigma_T\sin\phi}{r\cos^2\phi}\dot{\phi} + \frac{V\cos\theta_T\cos\sigma_T}{r^2\cos\phi}\dot{r}$$

Substituting the expression of $\ddot{\phi}$ and $\ddot{\lambda}$ into (28) produces

$$\begin{aligned} C^{(2)} &= M_1 + N_1\ddot{\phi} + N_2\ddot{\lambda} = M_1 + N_1\frac{\cos\theta_T\cos\sigma_T}{r}\dot{V} \\ &-N_1\frac{V\cos\theta_T\cos\sigma_T}{r^2}\dot{r} - N_2\frac{\cos\theta_T\cos\sigma_T}{r\cos\phi}\dot{V} \\ &-N_2\frac{V\cos\theta_T\cos\sigma_T\sin\phi}{r\cos^2\phi}\dot{\phi} + N_2\frac{V\cos\theta_T\cos\sigma_T}{r^2\cos\phi}\dot{r} \\ &+\left(N_2\frac{V\sin\theta_T\cos\sigma_T}{r\cos\phi} - N_1\frac{V\sin\theta_T\cos\sigma_T}{r}\right)\dot{\theta}_T \\ &+\left(N_2\frac{V\cos\theta_T\cos\sigma_T}{r\cos\phi} - N_1\frac{V\cos\theta_T\sin\sigma_T}{r}\right)\dot{\sigma}_T \end{aligned} \tag{29}$$

The first six parts of (29) are independent of bank angle and may be written as M_2; the coefficients before $\dot{\theta}_T$ and $\dot{\sigma}_T$ may be written as N_3 and N_4.

$$C^{(2)} = M_2 + N_3\dot{\theta}_T + N_4\dot{\sigma}_T \tag{30}$$

Combining with dynamic equations and substituting the expressions of $\dot{\theta}_T$ and $\dot{\sigma}_T$ into (30),

$$\begin{aligned} C^{(2)} &= M_2 + N_3(-g\cos\theta_T/V + V\cos\theta_T/r + \\ &+ (\cos\phi\sin\phi\cos\sigma_T\sin\theta_T + \cos^2\phi\cos\theta_T)\omega_e^2 r/V - 2\omega_e\cos\phi\sin\sigma_T) \\ &+ N_4(V\cos\theta_T\sin\sigma_T\tan\phi/r - \omega_e^2 r\cos\phi\sin\phi\sin\sigma_T/(V\cos\theta_T) \\ &+ 2(\cos\sigma_T\sin\theta_T\cos\phi - \sin\phi\cos\theta_T)\omega_e/\cos\theta_T) \\ &+ N_3\frac{Y}{mV}\cos\gamma_v - N_4\frac{Y}{mV\cos\theta_T}\sin\gamma_v \end{aligned}$$

Substituting the expressions of $C^{(2)}$ into (26) produces

$$\begin{aligned} S_w^{(2)} &= -R\frac{1}{\sqrt{1-C^2}}M_2 - R\frac{1}{\sqrt{1-C^2}}N_3(-g\cos\theta_T/V + V\cos\theta_T/r + \\ &+ (\cos\phi\sin\phi\cos\sigma_T\sin\theta_T + \cos^2\phi\cos\theta_T)\omega_e^2 r/V \\ &-2\omega_e\cos\phi\sin\sigma_T) - R\frac{1}{\sqrt{1-C^2}}N_4(V\cos\theta_T\sin\sigma_T\tan\phi/r \\ &-\omega_e^2 r\cos\phi\sin\phi\sin\sigma_T/(V\cos\theta_T) \\ &+ 2(\cos\sigma_T\sin\theta_T\cos\phi - \sin\phi\cos\theta_T)\omega_e/\cos\theta_T) \\ &-N_3R\frac{1}{\sqrt{1-C^2}}\frac{Y}{mV}\cos\gamma_v + N_4R\frac{1}{\sqrt{1-C^2}}\frac{Y}{mV\cos\theta_T}\sin\gamma_v \end{aligned}$$

The first three parts of the equation above are independent of bank angle and may be written as M_3; the coefficients before $\cos\gamma_v$ and $\sin\gamma_v$ may be denoted N_5 and N_6

$$S_w^{(2)} = M_3 + N_5\cos\gamma_v + N_6\sin\gamma_v = 0 \tag{31}$$

By solving the equation above, we may obtain the command for the bank angle

$$\gamma_v = -2 * \arctan\left(\left(N_6 + \sqrt{-M_3^2 + N_5^2 + N_6^2}\right)\Big/(M_3 - N_5)\right) \tag{32}$$